[Peroxotetraphenylporphinato]manganese(III) and [Chlorotetraphenylporphinato]manganese(II) Anions. Syntheses, Crystal Structures, and Electronic Structures

Reuel B. VanAtta,[†] Charles E. Strouse,[†] Louise Karle Hanson,[‡] and Joan Selverstone Valentine*[†]

Contribution from the Department of Chemistry and Biochemistry and Molecular Biology Institute, University of California, Los Angeles, Los Angeles, California 90024, and Division of Chemical Science, Department of Applied Science, Brookhaven National Laboratory, Upton, New York 11973. *Received July 3, 1986*

Abstract: The syntheses and X-ray crystal structures of potassium cryptate $[K(K222)]^+$ salts of the [chlorotetraphenylporphinato]manganese(II) and [peroxotetraphenylporphinato]manganese(III) anions are reported. The complexes are prepared in THF by reaction of $Mn^{II}TPP$ with Cl^- and O_2^-, respectively. Both complexes crystallize in the space group $P2_1/c$ with four formula units per unit cell. The unit cell of the chloride complex has dimensions a = 12.834 Å, b = 18.999 Å, c = 23.313 Å, β = 99.02 at 133 K. The least-squares refinement led to final values of R = 0.062 and R_w = 0.066. The manganese is pentacoordinate, bonded to four pyrrole nitrogens and a chloride ion. The manganese atom is displaced 0.641 Å from the least-squares plane based on the four pyrrole nitrogen atoms in the direction of the chloride ligand. The unit cell of the manganese(III)-peroxo complex has dimensions a = 12.895 Å, b = 18.836 Å, c = 23.045 Å, β = 99.17 at 133 K. The least-squares refinement led to final values of R = 0.057 and R_w = 0.067. The manganese is bonded to four pyrrole nitrogens and the bidentate peroxo ligand. The manganese lies 0.764 Å above the least-squares plane based on the pyrrole nitrogens toward the peroxo ligand. The O-O bond distance is 1.421 (5) Å, and the Mn-O distances are 1.901 (4) and 1.888 (4) Å. The peroxo ligand is bound "side-on" to the manganese, eclipsing two of the manganese-pyrrole nitrogen bonds. The binding of dioxygen as peroxide was unexpected because the NMR and optical spectra of $[Mn^{III}TPPO_2]^-$ are typical of a manganese(II)- not a manganese(III)-porphyrin complex. Charge iterative extended Hückel calculations show that the strong bonding between the peroxide and the manganese, coupled with the large manganese out-of-plane displacement, leads to an alteration of the d orbital ordering: the highest energy d orbital is a $d_{yz} + O_2\pi_{gz}$ hybrid, not the usual $d_{x^2-y^2}$. This result reconciles the seemingly contradictory spectroscopic and crystallographic data. Occupation of the $d_{x^2-y^2}$ orbital is consistent with both the large out-of-plane displacement of the Mn atom and the NMR spectra. The high energy of the hybrid $d_{yz} + O_2\pi_{gz}$ orbital accounts for the lack of multiple Soret bands in the optical spectra.

A primary goal in the study of heme-containing enzymes is an accurate description of the binding of dioxygen (and species derived from it) to iron throughout the course of the catalytic reaction. Dioxygen complexes of metalloporphyrins provide structural analogues of dioxygen complexes that may be involved in the reactions of these enzymes. In the case of the monooxygenase enzyme cytochrome P450, for example, spectroscopic evidence indicates that dioxygen is bound initially in a fashion similar to that found for oxymyoglobin. Analogues for this intermediate have previously been synthesized by reaction of Fe(II) porphyrins with dioxygen.[1] The dioxygen ligand in such complexes binds in an end-on fashion which is "superoxo-like" when compared with other characterized metal-dioxygen complexes.

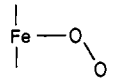

After formation of the initial dioxygen complex in the cytochrome P450 mechanism, the enzyme is reduced, presumably forming an intermediate at the same oxidation level as an iron(III) peroxide or hydroperoxide complex. This intermediate has never been observed, however, because the subsequent O-O bond cleavage and formation of high-valent iron-oxo intermediates are very fast.

The absence of observable cytochrome P450 intermediates in which the dioxygen ligand is at the peroxide, i.e., O_2^{2-}, oxidation level makes synthetic analogues of particular interest. Several years ago, McCandlish et al.[2] reported the synthesis and characterization of a ferric porphyrin-peroxo complex. This complex was prepared by reaction of FeTPPCl with 2 equiv of superoxide anion, O_2^-. The first equivalent was found to reduce $Fe^{III}TPPCl$ to $Fe^{II}TPP$. Addition of the second equivalent produced what was formulated as $[Fe^{III}TPPO_2]^-$. This species was characterized by visible absorption spectroscopy, ESR, and IR with isotopic (^{18}O) labeling. On the basis of those spectroscopic results, the dioxygen ligand was predicted to be peroxide, bound in a side-on, bidentate fashion. EXAFS studies appear to support this conclusion.[3]

Since that time, other groups have generated the species by alternative methods. Reed et al.[4] obtained the same product by reacting $Fe^{I}TPP^-$ with O_2 and Dolphin[5] by electrochemically reducing $Fe^{II}TPPO_2$ by one electron. We and other groups have attempted to crystallize this complex in order to carry out an X-ray crystal structural determination. Although we have recently succeeded in crystallizing this complex and characterizing the solid,[6] crystals suitable for a structural study have not yet been obtained. A parallel study using manganese porphyrins[7] revealed that MnTPPCl undergoes a similar two-step reaction with superoxide. MnTPPCl is first reduced by 1 equiv of superoxide to give $Mn^{II}TPP$, which reacts further with a second equivalent of

[†] University of California, Los Angeles.
[‡] Brookhaven National Laboratory.

(1) (a) Collman, J. P.; Brauman, J. I.; Halbert, T. R.; Suslick, K. S. *Proc. Natl. Acad. Sci. U.S.A.* **1976**, *73*, 3333. (b) Collman, J. P.; Gagne, R. R.; Reed, C. A.; Robinson, W. T.; Rodley, G. A. *Proc. Natl. Acad. Sci. U.S.A.* **1974**, *71*, 1326.
(2) McCandlish, E.; Miksztal, A. R.; Nappa, M.; Sprenger, A. Q.; Valentine, J. S.; Stong, J. D.; Spiro, T. G. *J. Am. Chem. Soc.* **1980**, *102*, 4268.
(3) Friant, P.; Goulon, J.; Fischer, J.; Ricard, L.; Schappacher, M.; Weiss, R.; Momenteau, M. *Nouv. J. Chim.* **1985**, *9*, 33.
(4) Reed, C. A. In *Electrochemical and Spectrochemical Studies of Biological Redox Components*; Kadish, K. M., Ed.; Advances in Chemistry 201; American Chemical Society: Washington, DC, 1982; pp 333-356.
(5) Welborn, C. H.; Dolphin, D.; James, B. R. *J. Am. Chem. Soc.* **1981**, *103*, 2869.
(6) Burstyn, J. N.; Miksztal, A. R.; Roe, J. A.; Shaevitz, B.; Lang, G.; Valentine, J. S., manuscript in preparation.
(7) Valentine, J. S.; Quinn, A. E. *Inorg. Chem.* **1976**, *15*, 1997.

0002-7863/87/1509-1425$01.50/0 © 1987 American Chemical Society

superoxide to yield a product, $[MnTPP(O_2)]^-$, believed to be either a manganese(II) superoxide or a manganese(III) peroxide complex. Shirazi and Goff[8] subsequently studied this complex by deuterium NMR and observed a downfield shift of the pyrrole hydrogens. Such shifts had been shown to be characteristic of an unpaired electron in the $d_{x^2-y^2}$ orbital. Since for metalloporphyrin transition metal complexes this d orbital is usually highest in energy, these authors concluded that the manganese must be d^5, i.e., Mn(II).

Here we report the results of X-ray crystallographic studies of [K(K222)][$MnTPPO_2$], **1**, and of the structurally related Mn(II) complex [K(K222)][MnTPPCl], **2**. The geometry of binding of the dioxygen ligand and the O–O bond distance in **1** positively establish that the ligand is peroxide. If dioxygen is bound to the complex as peroxide, O_2^{2-}, we are forced to conclude that manganese is in the 3+ oxidation state. This surprising result apparently conflicts with the NMR results of Shirazi and Goff. Moreover, the structures of **1** and **2** are remarkably similar in spite of the difference in the oxidation states of manganese. In an effort to explain these results, charge iterative extended Hückel (IEH) calculations were performed on both **1** and **2**. The results of these calculations provide a satisfactory resolution of the apparent contradictions.

Experimental Section

Materials. Tetrahydrofuran (THF) and toluene were distilled from sodium benzophenone. MnTPPCl was prepared as described previously.[9] Kryptofix (K222) (4,7,13,16,21,24-hexaoxa-1,10-diazabicyclo[8.8.8]-hexacosane) was purchased from MCB Reagents, dried over P_2O_5, and sublimed. Potassium superoxide was purchased from Alfa (96.5%, small chunks) and used without further purification. Zinc amalgam was prepared by literature methods[10] and dried by heating under vacuum. A Vacuum Atmospheres inert atmosphere chamber containing helium was used to store all materials and to carry out reactions.

Instrumentation. Visible spectra were recorded on a Beckman 5270 spectrophotometer. Crystallographic data were collected on Syntex and Picker diffractometers. All data analysis made use of the UCLA crystallographic computation package with DEC-VAX computers.[11]

Synthesis of [K(222)][MnTPPCl], 2. An initial attempt to synthesize the manganese(III)–peroxide complex yielded the manganese(II)–chloride complex instead. In an inert atmosphere box, $Mn^{III}TPPCl$ (5 mg) was dissolved in THF (2 mL). A small amount of zinc amalgam was added, and the solution was stirred until the color changed from green to blue and the visible absorption spectrum showed the solution to contain only $Mn^{II}TPP$. The solid zinc amalgam was removed by filtering the solution into a test tube through a Gelman Acrodisc 0.45 μ filter (PTFE) attached to a 5-mL syringe. A fourfold excess of K222 was added to the $Mn^{II}TPP$ solution along with several small pieces of KO_2 (2–3 mm in diameter). The test tube was stoppered and left for several days. During this period, the solution color changed from blue to green and eventually became pale as green crystals deposited on the KO_2 chunks and on the glass walls of the test tube. Some of the latter were suitable for X-ray crystallography.

Synthesis of [K(K222)][$MnTPPO_2$], 1. The manganese–peroxo complex was synthesized in a manner similar to that described above. In order to eliminate chloride ion from the solution, MnTPPCl was first reduced by stirring with zinc amalgam in toluene. The solution was filtered to remove the zinc amalgam and the insoluble KCl, and the toluene was removed by vacuum distillation. The resulting $Mn^{II}TPP$ was redissolved in THF, and the procedure described above for the synthesis of **2** was followed.

X-ray Structure Determination. A summary of crystallographic parameters for **1** and **2** is given in Table I. A crystal of **2** was mounted on a Syntex $P\bar{1}$ diffractometer, and data were collected at −140 °C. The complex **2** was found to have crystallized in the space group $P2_1/c$ with four formula units per unit cell. Analytical, difference Fourier, and least-squares refinement techniques were used to locate all non-hydrogen atoms. Positions of all hydrogen atoms were calculated based on idealized bond lengths, and their positions were held constant during subsequent refinements. Positions of all the non-hydrogen atoms were refined along with the anisotropic thermal parameters of the chloride, the cryptate (K222), and the carbon atoms of two of the porphyrin phenyl rings. A final least-squares refinement led to $R = 0.062$, $R_w = 0.066$. The data-to-parameter ratio is 9.13, and the error of fit is 1.5089. The data for the structure of **1** were collected and analyzed in the same manner with the exception that a Picker diffractometer was used for data collection. Positions of all non-hydrogen atoms were refined along with the anisotropic thermal parameters for manganese, the potassium cryptate anion, the peroxo ligand, and the carbon atoms of all four porphyrin phenyl rings. The final refinement led to $R = 0.057$, $R_w = 0.067$. The data-to-parameter ratio is 8.62, and the error of fit is 1.7567.

Table I. Experimental Parameters

formula	$C_{62}H_{64}N_6O_6KClMn$	$C_{62}H_{64}N_6O_8KMn$
Z	4	4
a	12.834 (2) Å	12.895 (1) Å
b	18.999 (3) Å	18.836 (3) Å
c	23.313 (3) Å	23.045 (3) Å
β	99.02 (1)°	99.17 (1)°
radiation	Mo $K\alpha$ (cryst monochromtzd)	0.71069 Å
temp °C	−140	−140
space group	$P2_1/c$	$P2_1/c$
cryst dimensions	0.16 × 0.20 × 0.30 mm	0.19 × 0.27 × 0.41 mm
diffractometer	Syntex	Picker
scan speed (deg/min)	6	6
scan technique	$\theta/2\theta$	$\theta/2\theta$
2θ (max)	50°	50°
data collctd	$h,k,\pm l$	$h,k,\pm l$
no. of data measd	10748	10559
no. of data obsd with $[I>3\sigma(I)]$	4601	5027
R	0.062	0.057
R_w	0.066	0.067

Table II. Coordinates Used in the $[MnPL]^-$ Calculations

	square $[MnPCl]^-$ or $[MnPO_2]^-$			rectangular $[MnPO_2]^-$		
atom[a]	x	y	z	x	y	z
H_b	1.312	5.133	0.0	1.312	5.066	0.0
C_b	0.675	4.260	0.0	0.675	4.193	0.0
C_a	1.114	2.881	0.0	1.114	2.814	0.0
C_m	2.440	2.440	0.0	2.445	2.427	0.0
H_m	3.203	3.203	0.0	3.208	3.190	0.0
C_a	2.881	1.114	0.0	2.906	1.114	0.0
C_b	4.260	0.675	0.0	4.285	0.675	0.0
H_b	5.133	1.312	0.0	5.158	1.312	0.0
N_y	0.0	2.065	0.0	0.0	1.998	−0.074
N_x	2.065	0.0	0.0	2.090	0.0	0.074
Mn	0.0	0.0	0.641[b]	0.0	0.0	0.762[c]
O				0.0	0.710	2.518[c]
Cl	0.0	0.0	3.006[b]			

[a] Coordinates are given for one quadrant of the molecule. [b] Mn,Cl coordinates used for the $[MnPCl]^-$ calculations. [c] Mn,O coordinates used for the $[MnPO_2]^-$ calculations (square and rectangular porphyrins).

Theoretical Calculations. These were performed by the charge iterative extended Hückel[12] (IEH) and INDO/s[13] methods. The programs and parameters have been previously described. The atomic coordinates were based upon the crystal structure results and are given in Table II. Porphine (P) rather than tetraphenylporphine (TPP) macrocycles were used for the calculated complexes.

IEH contains only one-center terms and converges on charge density. The method has a long history of application to metalloporphyrins and provides readily interpretable molecular orbitals (MO's). The INDO/s method includes two-center repulsion integrals and converges on total energy. When used in the UHF (unrestricted Hartree–Fock) mode for open-shelled systems, the resultant INDO MO's are less interpretable

(8) Shirazi, A.; Goff, H. M. *J. Am. Chem. Soc.* **1982**, *104*, 6318.
(9) Alder, A. D.; Longo, F. R.; Kampas, F.; Kim, J. *J. Inorg. Nucl. Chem.* **1970**, *32*, 2443.
(10) Gordon, A. J.; Ford, R. A. *A Chemists Companion*; J. Wiley and Son: New York, 1972; p 438.
(11) Scattering factors and anomalous dispersion corrections were taken from *International Tables for X-ray Crystallography*; Kynoch: Birmingham, England, 1974.
(12) (a) Schaffer, A. M.; Gouterman, M.; Davidson, E. R. *Theor. Chim. Acta* **1973**, *30*, 9. (b) Zerner, M.; Gouterman, M. *Ibid.* **1966**, *4*, 44. (c) Zerner, M.; Gouterman, M.; Kobayashi, H. *Ibid.* **1966**, *6*, 363.
(13) (a) Ridley, J. E.; Zerner, M. C. *Theor. Chim. Acta* **1973**, *32*, 111. (b) Ridley, J. E.; Zerner, M. C. *Ibid.* **1976**, *42*, 223. (c) Bacon, A. D.; Zerner, M. C. *Ibid.* **1979**, *53*, 21.

Table III. Fractional Atomic Coordinates for [MnTPPCl]]K(K222)][a]

atom	x	y	z	atom	x	y	z
C(1)	0.7276 (5)	0.3100 (4)	0.1427 (3)	C(52)	0.4712 (5)	0.3676 (4)	0.0894 (3)
C(2)	0.7767 (5)	0.3591 (4)	0.1079 (3)	C(53)	0.4073 (6)	0.3962 (4)	0.0415 (4)
C(3)	0.8788 (5)	0.3668 (4)	0.1324 (3)	C(54)	0.4207 (7)	0.3774 (6)	−0.0138 (4)
C(4)	0.8933 (5)	0.3228 (4)	0.1842 (3)	C(55)	0.5009 (7)	0.3320 (5)	−0.0218 (3)
C(5)	0.9874 (5)	0.3173 (4)	0.2245 (3)	C(56)	0.5668 (6)	0.3040 (4)	0.0256 (3)
C(6)	1.0011 (5)	0.2778 (3)	0.2754 (3)	C(61)	0.6990 (9)	0.3133 (5)	0.3617 (4)
C(7)	1.0960 (5)	0.2777 (4)	0.3187 (3)	C(62)	0.7112 (9)	0.3060 (5)	0.4265 (5)
C(8)	1.0786 (5)	0.2352 (4)	0.3616 (3)	C(63)	0.8098 (11)	0.3514 (6)	0.5133 (5)
C(9)	0.9728 (5)	0.2070 (3)	0.3462 (3)	C(64)	0.8698 (8)	0.4122 (8)	0.5394 (4)
C(10)	0.9248 (5)	0.1601 (3)	0.3808 (3)	C(65)	0.8528 (7)	0.5275 (6)	0.5692 (4)
C(11)	0.8183 (5)	0.1381 (3)	0.3699 (3)	C(66)	0.7796 (8)	0.5899 (5)	0.5629 (4)
C(12)	0.7672 (5)	0.1002 (4)	0.4111 (3)	C(71)	0.5287 (10)	0.3650 (6)	0.3331 (4)
C(13)	0.6645 (5)	0.0940 (4)	0.3876 (3)	C(72)	0.4622 (7)	0.4295 (6)	0.3252 (4)
C(14)	0.6530 (5)	0.1270 (3)	0.3306 (3)	C(73)	0.4249 (6)	0.5348 (5)	0.3698 (5)
C(15)	0.5554 (5)	0.1366 (3)	0.2925 (3)	C(74)	0.4388 (6)	0.5726 (5)	0.4264 (6)
C(16)	0.5435 (5)	0.1753 (3)	0.2406 (3)	C(75)	0.5618 (7)	0.6305 (5)	0.4957 (5)
C(17)	0.4437 (5)	0.1815 (4)	0.2008 (3)	C(76)	0.6667 (7)	0.6677 (4)	0.5003 (4)
C(18)	0.4626 (5)	0.2248 (4)	0.1569 (3)	C(81)	0.6736 (7)	0.3971 (5)	0.2839 (3)
C(19)	0.5717 (5)	0.2438 (4)	0.1687 (3)	C(82)	0.7810 (7)	0.4285 (5)	0.2882 (3)
C(20)	0.6208 (5)	0.2892 (3)	0.1333 (3)	C(83)	0.8779 (6)	0.5328 (4)	0.3154 (3)
C(21)	1.0815 (5)	0.3582 (4)	0.2116 (3)	C(84)	0.8688 (5)	0.6046 (4)	0.3400 (3)
C(22)	1.0864 (5)	0.4307 (4)	0.2150 (3)	C(85)	0.8482 (6)	0.6662 (4)	0.4250 (4)
C(23)	1.1755 (6)	0.4670 (4)	0.2046 (4)	C(86)	0.8507 (6)	0.6576 (5)	0.4891 (3)
C(24)	1.2589 (6)	0.4305 (5)	0.1897 (3)	N(1)	0.8007 (4)	0.2885 (3)	0.1886 (2)
C(25)	1.2560 (6)	0.3576 (5)	0.1859 (3)	N(2)	0.9277 (4)	0.2346 (3)	0.2938 (2)
C(26)	1.1678 (5)	0.3210 (4)	0.1970 (3)	N(3)	0.7486 (4)	0.1529 (3)	0.3212 (2)
C(31)	0.9924 (5)	0.1316 (4)	0.4337 (3)	N(4)	0.6193 (4)	0.2128 (3)	0.2190 (2)
C(32)	1.0055 (5)	0.1661 (4)	0.4865 (3)	N(5)	0.6430 (6)	0.3778 (4)	0.3408 (3)
C(33)	1.0703 (6)	0.1374 (4)	0.5349 (3)	N(6)	0.7577 (5)	0.6196 (3)	0.5042 (3)
C(34)	1.1219 (6)	0.0758 (4)	0.5298 (3)	O(1)	0.7772 (6)	0.3611 (3)	0.4532 (3)
C(35)	1.1096 (6)	0.0395 (5)	0.4779 (4)	O(2)	0.8049 (4)	0.4717 (3)	0.5340 (2)
C(36)	1.0454 (6)	0.0679 (4)	0.4293 (3)	O(3)	0.4818 (4)	0.4704 (3)	0.3767 (2)
C(41)	0.4594 (5)	0.1052 (4)	0.3101 (3)	O(4)	0.5476 (4)	0.5912 (3)	0.4429 (3)
C(42)	0.3709 (5)	0.1464 (4)	0.3151 (3)	O(5)	0.7808 (4)	0.4963 (3)	0.3155 (2)
C(43)	0.2794 (5)	0.1166 (4)	0.3306 (3)	O(6)	0.8555 (4)	0.5988 (3)	0.3995 (2)
C(44)	0.2763 (5)	0.0456 (4)	0.3422 (3)	Cl	0.8450 (2)	0.1015 (1)	0.1878 (1)
C(45)	0.3640 (5)	0.0041 (4)	0.3395 (3)	K	0.7022 (1)	0.4986 (1)	0.4204 (1)
C(46)	0.4527 (5)	0.0342 (4)	0.3223 (3)	Mn	0.7873 (1)	0.1958 (1)	0.2411 (0)
C(51)	0.5529 (5)	0.3205 (4)	0.0816 (3)				

[a] Numbers in parentheses following atomic coordinates are estimated standard deviations.

Table IV. Selected Bond Lengths (Å) for [MnTPPCl][K(K222)][a]

Mn–Cl	2.364 (2)	C4–N1	1.373 (8)	C12–C13	1.351 (8)
Mn–N1	2.167 (5)	C5–C6	1.392 (8)	C13–C14	1.456 (9)
Mn–N2	2.146 (5)	C6–C7	1.455 (8)	C14–C15	1.429 (8)
Mn–N3	2.165 (5)	C6–N2	1.368 (8)	C14–N3	1.371 (7)
Mn–N4	2.161 (5)	C7–C8	1.331 (9)	C15–C16	1.404 (8)
C1–C2	1.444 (9)	C8–C9	1.451 (8)	C16–C17	1.464 (8)
C1–C20	1.410 (8)	C9–C10	1.407 (8)	C16–N4	1.364 (7)
C1–N1	1.370 (8)	C9–N2	1.371 (7)	C17–C18	1.364 (9)
C2–C3	1.353 (9)	C10–C11	1.414 (8)	C18–C19	1.430 (9)
C3–C4	1.456 (9)	C11–C12	1.438 (8)	C19–C20	1.409 (8)
C4–C5	1.413 (8)	C11–N3	1.360 (7)	C19–N4	1.368 (8)
K–O1	2.847 (6)	K–O4	2.763 (5)	K–N5	2.974 (7)
K–O2	2.814 (5)	K–O5	2.788 (5)	K–N6	3.029 (6)
K–O3	2.902 (5)	K–O6	2.834 (5)		

[a] Estimated standard deviations in parentheses.

than those of the IEH. However, INDO calculations provide much more reliable total energies.

Results

Structure of [K(K222)][MnTPPCl], 2. Figure 1 presents an ORTEP drawing and numbering scheme of the manganese porphyrin chloride anion and potassium cryptate cation. Figure 2 shows the perpendicular displacements of the atoms from the average plane derived from (A) the 24 atom porphyrin core and (B) the four pyrrole nitrogens. Table III lists the atomic coordinates. Tables IV and V list selected bond distances and bond angles of the porphyrin core, the potassium cryptate anion, and the chloride ligand. Figure 6 illustrates the manganese coordination.

Table VI lists the average manganese–nitrogen bond lengths and manganese out-of-plane displacements for a number of Mn(II)– and Mn(III)–porphyrin complexes. It can be seen that

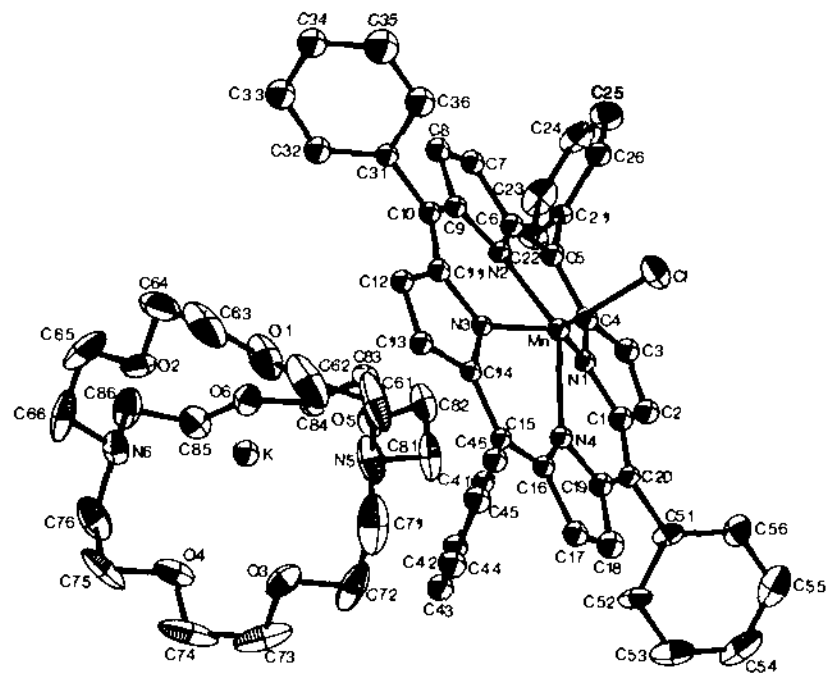

Figure 1. ORTEP plot of [K(K222)][MnTPPCl] showing both the porphyrin anion and potassium cryptate cation with the numbering scheme used in the text. Hydrogen atoms have been omitted for clarity.

the values determined for **2**, average Mn–N = 2.160 (10) Å and Ct–Mn = 0.641 Å, are large. (For distances reported as averages, the standard deviation is from the averaged value (assuming the same population).) For instance, the high spin, five-coordinate complex Mn^{II}TPP(1-methylimidazole)[14] has an average Mn–N bond length of 2.128 (7) Å and a manganese displacement of 0.512

(14) Kirner, J. F.; Reed, C. A.; Scheidt, W. R. *J. Am. Chem. Soc.* **1977**, *99*, 2557.

Table V. Selected Bond Angles (deg) for [MnTPPCl][K(K222)][a]

N1-Mn-C1	105.1 (2)	C5-C4-N1	125.1 (6)
N2-Mn-C1	104.9 (2)	C4-C5-C6	126.0 (6)
N3-Mn-C1	107.5 (2)	C5-C6-N2	126.1 (6)
N4-Mn-C1	111.8 (2)	C5-C6-C7	124.9 (6)
N1-Mn-N3	147.4 (2)	C7-C6-N2	108.9 (6)
N2-Mn-N4	143.3 (2)	C6-C7-C8	107.5 (6)
N1-Mn-N2	84.9 (2)	C7-C8-C9	107.4 (6)
N2-Mn-N3	85.5 (2)	C8-C9-N2	109.1 (6)
N3-Mn-N4	84.7 (2)	C8-C9-C10	124.7 (6)
N4-Mn-N1	84.8 (2)	C10-C9-N2	126.2 (6)
C1-N1-Mn	125.3 (4)	C9-C10-C11	125.6 (6)
C1-N1-C4	107.2 (5)	C10-C11-N3	125.4 (6)
C4-N1-Mn	125.0 (4)	C10-C11-C12	123.9 (6)
C6-N2-Mn	125.7 (4)	C12-C11-N3	110.6 (6)
C6-N2-C9	107.1 (5)	C11-C12-C13	106.9 (6)
C9-N2-Mn	125.3 (4)	C12-C13-C14	106.6 (6)
C11-N3-Mn	126.0 (4)	C13-C14-N3	109.6 (5)
C11-N3-C14	106.3 (5)	C13-C14-C15	126.2 (6)
C14-N3-Mn	127.2 (4)	C15-C14-N3	125.0 (6)
C16-N4-Mn	125.2 (4)	C14-C15-C16	124.7 (6)
C16-N4-C19	107.0 (5)	C15-C16-N4	127.2 (6)
C19-N4-Mn	124.3 (4)	C15-C16-C17	123.7 (6)
C20-C1-N1	124.6 (6)	C17-C16-N4	109.1 (6)
C20-C1-C2	126.4 (6)	C16-C17-C18	106.5 (6)
C2-C1-N1	109.0 (6)	C17-C18-C19	107.0 (6)
C1-C2-C3	108.2 (6)	C18-C19-N4	110.4 (6)
C2-C3-C4	106.1 (6)	C18-C19-C20	123.8 (6)
C3-C4-N1	109.6 (6)	C20-C19-N4	125.8 (6)
C3-C4-C5	125.4 (6)	C19-C20-C1	126.4 (6)

[a] Estimated standard deviations in parentheses.

Table VI. Comparison of Some Manganese Porphyrins

	out-of-plane dist	av Mn-N dist[f]
$Mn^{II}TPP$[a]		2.084 (2)
$Mn^{II}TPP(NO)$[b]	0.34	2.004 (5)
$Mn^{II}TPP(1\text{-MeIm})$	0.512	2.128 (7)
$Mn^{II}TPP(Cl)^-$	0.641	2.160 (10)
$Mn^{III}TPP(Cl)$	0.27	2.009 (15)
$Mn^{III}TPP(CN)$[d]	0.25[c]	2.008 (8)
$Mn^{III}TPP(N_3)$[e]	0.234	2.005 (6)
$Mn^{III}TPP(O_2)^-$	0.764	2.184 (23)

[a] Four coordinate. [b] Low spin. [c] Displacement from porphinato core. [d] Reference 25. [e] Reference 26. [f] Standard deviations are from averaged value (assuming the same population).

Å. Values for the low spin MnTPP(NO)[15] and the four-coordinate high spin $Mn^{II}TPP$[16] are even smaller.

A closely related complex, [*N*-methyltetraphenylporphinato]-manganese(II) chloride,[17] has a structure that resembles that of **2**. $Mn^{II}(N\text{-}CH_3TPP)Cl$ has one long manganese–nitrogen bond (2.368 (5) Å) to the methylated pyrrole nitrogen, but the other distances average 2.143 (22) Å, similar to those of **2**. The out-of-plane distance (plane containing the three nonmethylated pyrrole nitrogens) is 0.689 Å, again similar to the distance of 0.641 Å for $[MnTPPCl]^-$. However, a direct comparison of these two complexes may not be appropriate since methylation of the pyrrole nitrogen perturbs the porphyrin ring and consequently alters the Mn–N bonding.[18]

The average Mn–N distance and Mn out-of-plane displacement for $Mn^{III}TPPCl$[19] are 2.009 (15) and 0.27 Å, respectively, significantly smaller than those of $[Mn^{II}TPPCl]^-$. This is not surprising since the d^4, $Mn^{III}TPPCl$ complex has an unoccupied $d_{x^2-y^2}$ orbital. $Fe^{III}TPPCl$,[20] which is isoelectronic with **2**, has an Fe–N

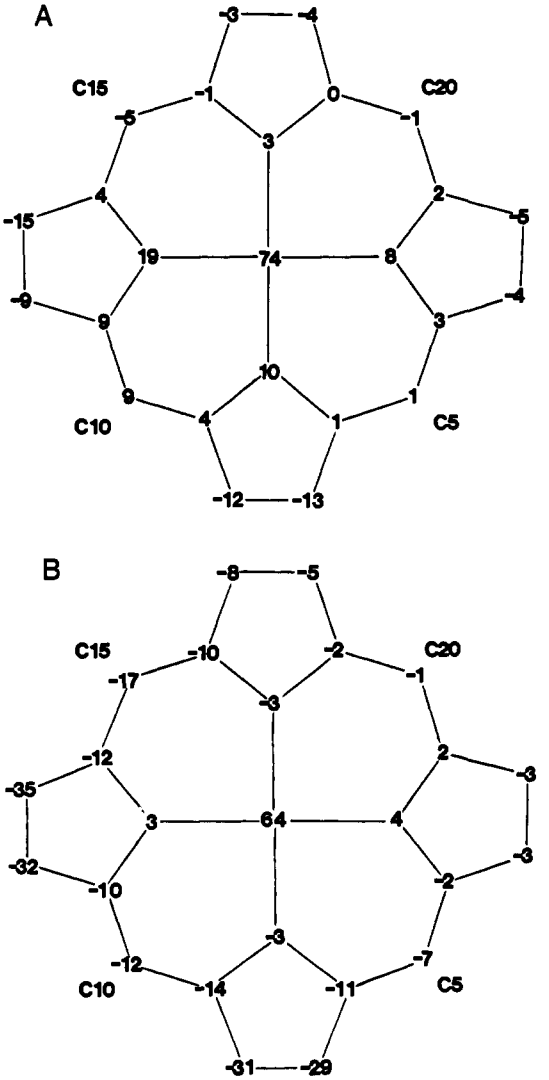

Figure 2. Displacement in units of 0.01 Å from the mean plane of (A) the 24 atom porphyrin core and (B) the four pyrrole nitrogens for $[MnTPPCl]^-$.

distance and iron displacement of 2.049 (9) and 0.383 Å, respectively. The longer metal–nitrogen bond length and metal out-of-plane displacement of **2** presumably reflects the larger ionic radius of Mn(II), due in part to its decreased charge relative to Fe(III).

The Mn–Cl distance in **2** is 2.364 (2) Å, and the Mn–Cl bond is slightly tilted (3.7°) from the pyrrole nitrogen plane toward N2. Even though the manganese of **2** differs in oxidation state, the Mn–Cl distance is almost exactly the same (2.363 (3) Å) as that of $Mn^{III}TPPCl$.[19] This observation can be explained if the additional electron in **2** is assumed to occupy the $d_{x^2-y^2}$ orbital (see Discussion below), since that orbital has little direct interaction with the axial ligand. Interestingly, the Mn–Cl distance is substantially shorter (2.295 (3) Å) for $Mn(NCH_3TPP)Cl$[17] than for **2** (2.364 (2) Å), possibly because differences in the bonding of the N-methylated porphyrin to manganese lead to increased interaction with the axial ligand.

The porphyrin ligand in **2** is found to be substantially domed (Figure 2), with the manganese atom and the four nitrogen atoms well out of the plane of the 24 atom porphyrin core. This is markedly different than the saddle shape found in $Mn^{III}TPPCl$[19] or $Mn^{II}TPP(NO)$.[15]

The counterion to the negatively charged porphyrin complex is a potassium cation chelated inside a "football" shaped cryptate,

(15) Scheidt, W. R.; Hatano, K.; Rupprecht, G. A.; Piciulo, P. L. *Inorg. Chem.* **1979**, *18*, 292.
(16) Kirner, J. F.; Reed, C. A.; Scheidt, W. R. *J. Am. Chem. Soc.* **1977**, *99*, 1093.
(17) Anderson, O. P.; Lavallee, D. K. *Inorg. Chem.* **1977**, *16*, 1634.
(18) Anderson, O. P.; Kopelove, A. B.; Lavallee, D. K. *Inorg. Chem.* **1980**, *19*, 2101.
(19) Tulinsky, A.; Chen, B. M. L. *J. Am. Chem. Soc.* **1977**, *99*, 3647.
(20) Hoard, J. L.; Cohen, G. H.; Glick, M. D. *J. Am. Chem. Soc.* **1967**, *89*, 1992.

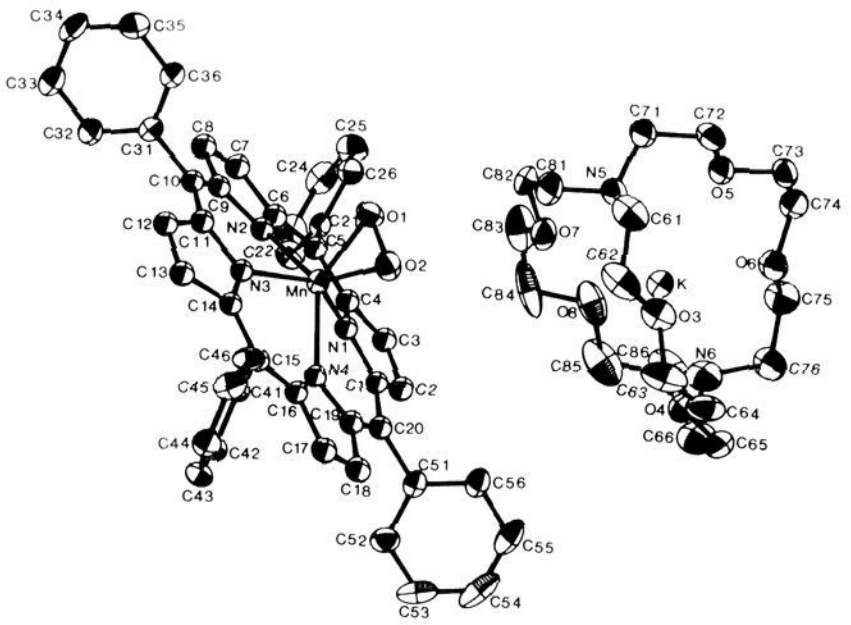

Figure 3. ORTEP plot of [K(K222)][$MnTTPO_2$] showing both the porphyrin anion and potassium cryptate cation with the numbering scheme used in the text. Hydrogen atoms have been omitted for clarity.

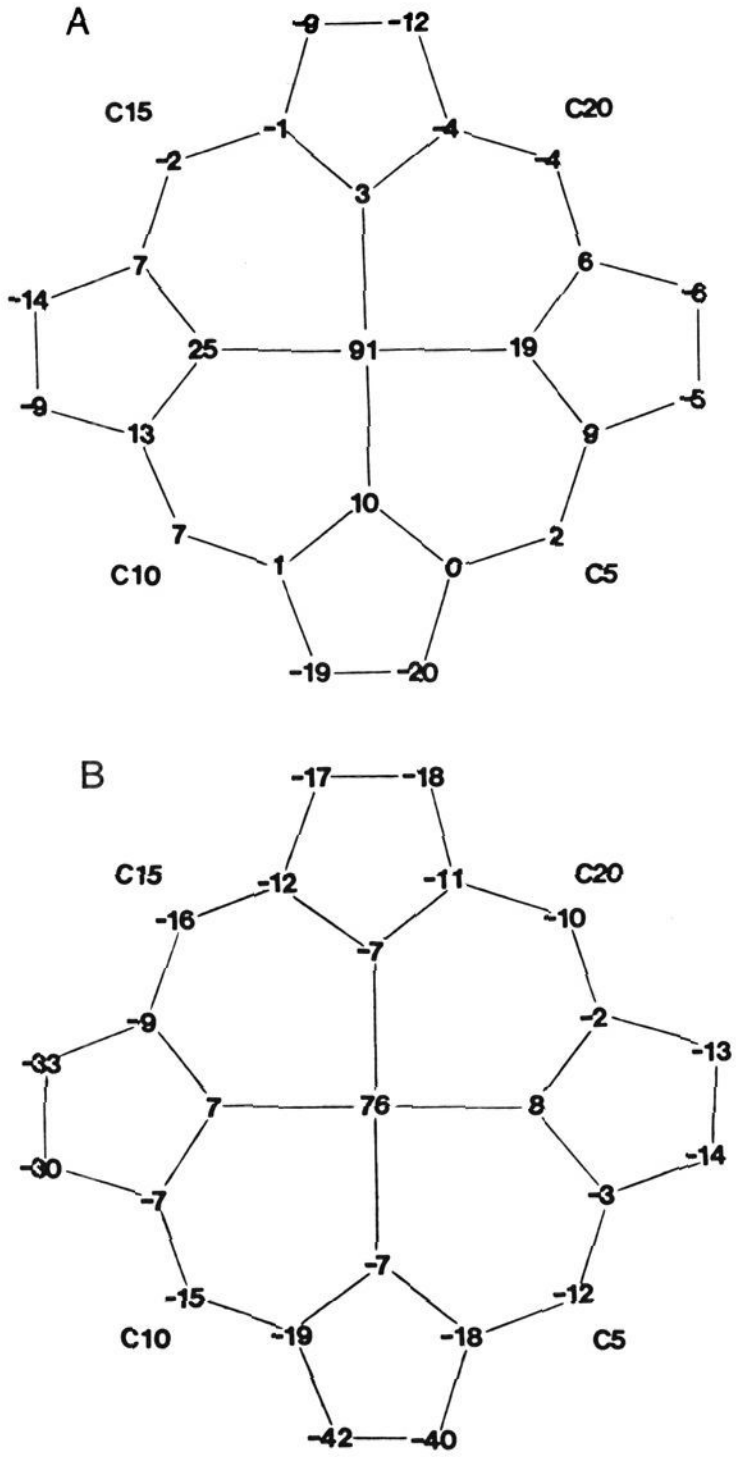

Figure 4. Displacement in units of 0.01 Å from the mean plane of (A) the 24 atom porphyrin core and (B) the four pyrrole nitrogens for [$MnTTPO_2$]$^-$.

K222, containing six oxygens and two nitrogens which point toward the potassium cation, binding it through electrostatic interactions. The K–O and K–N distances (see Table IV) which average 2.825 (49) and 3.002 (39) Å, respectively, are similar to those of the Mn–peroxo complex **1** and other published structures,[21] as are the other atomic distances (average): C–C = 1.493 (12), C–O = 1.422 (10), C–N = 1.474 (9) Å.

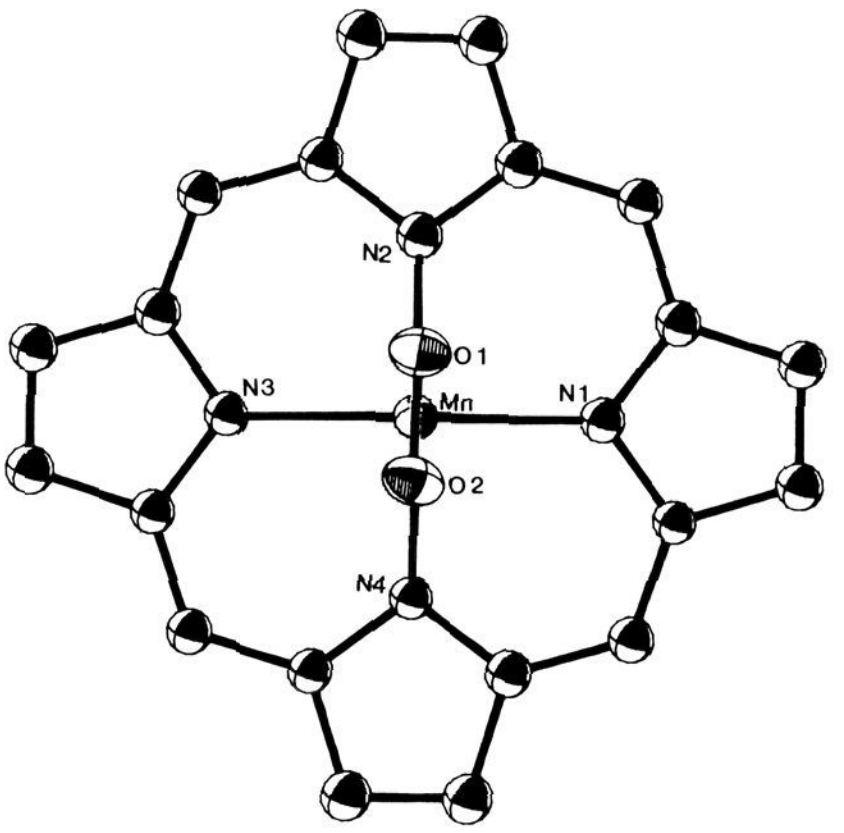

Figure 5. Top view of the porphyrin core with the dioxygen bound in a side-on fashion to the manganese center, eclipsing the N2 and N4 pyrrole nitrogens.

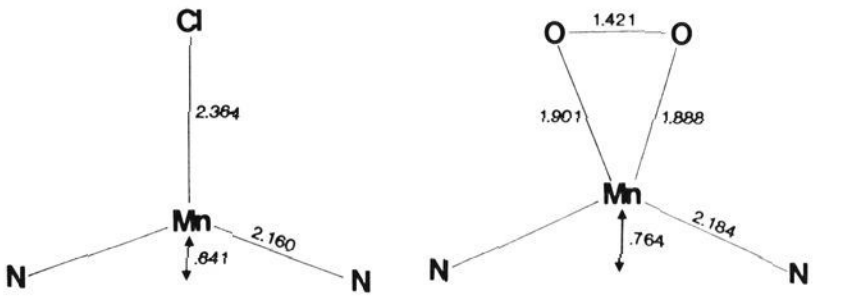

Figure 6. A schematic diagram comparing the two anions [MnTPPCl]$^-$ and [$MnTPPO_2$]$^-$. The out-of-plane distances are based on a plane containing the four pyrrole nitrogens. The distance given along the Mn–N bond represents the average value.

Structure of [K(K222)][$MnTPPO_2$], 1. Figure 3 presents an ORTEP diagram and numbering scheme of the porphyrin anion and potassium cryptate cation. Figure 4 gives the perpendicular displacements of the atoms from the average plane derived from (A) the 24 atom porphyrin core and (B) the four pyrrole nitrogens. Table VII lists the atomic coordinates. Tables VIII and IX list selected bond distances and angles of the porphyrin and ligand. Figure 5 is a top view of the porphyrin showing the orientation of the peroxo ligand. Figure 6 compares selected bond distances and the Mn out-of-plane distance for **1** and **2**.

It can be seen from Figure 3 that the dioxygen ligand is coordinated to the manganese in a side-on fashion, thus resembling known peroxo complexes rather than known superoxo complexes.[22] One might have predicted on steric grounds that the peroxo ligand would have preferred to bind to the manganese in a staggered configuration with respect to the four pyrrole nitrogens. However, as can be seen in Figure 5, the O_2^{2-} is found to eclipse N2 and N4. N2 and N4 lie 0.061 and 0.049 Å from the plane defined by Mn, O1, and O2. This structure thus resembles those of the two other structurally characterized metalloporphyrin–peroxo complexes, $TiOEPO_2$[23] and $MoTTP(O_2)_2$,[24] both of which bind

(21) (a) Quinn, R.; Strouse, C. E.; Valentine, J. S. *Inorg. Chem.* **1983**, *22*, 3934. (b) Miksztal, A. R. Ph.D. Thesis, Rutgers University, New Brunswick, NJ, 1985.

(22) (a) Valentine, J. S. *Chem. Rev.* **1973**, *73*, 235. (b) Vaska, L. *Acc. Chem. Res.* **1976**, *9*, 175.

(23) (a) Guilard, R.; Fontesse, M.; Fournari, P.; Lecomte, C.; Protas, J. *J. Chem. Soc., Chem. Commun.* **1976**, 161. (b) Guilard, R.; Latour, J.-M.; Lecomte, C.; Marchon, J.-C.; Protas, J.; Ripoll, D. *Inorg. Chem.* **1978**, *17*, 1228.

Table VII. Fractional Atomic Coordinates for $[MnTPPO_2][K(K222)]$[a]

atom	x	y	z	atom	x	y	z
C(1)	0.7738 (4)	0.3108 (3)	0.3645 (2)	C(53)	1.0946 (5)	0.4096 (4)	0.4560 (4)
C(2)	0.7261 (4)	0.3629 (3)	0.3987 (2)	C(54)	1.0875 (6)	0.3935 (4)	0.5134 (3)
C(3)	0.6250 (4)	0.3685 (3)	0.3738 (2)	C(55)	1.0140 (6)	0.3468 (4)	0.5255 (3)
C(4)	0.6080 (4)	0.3202 (3)	0.3239 (2)	C(56)	0.9450 (5)	0.3156 (3)	0.4801 (2)
C(5)	0.5169 (4)	0.3149 (3)	0.2832 (2)	C(61)	0.8294 (6)	-0.1678 (3)	0.5017 (3)
C(6)	0.5052 (4)	0.2746 (3)	0.2312 (2)	C(62)	0.9363 (6)	-0.1318 (4)	0.5102 (3)
C(7)	0.4130 (4)	0.2753 (3)	0.1873 (2)	C(63)	1.0526 (5)	-0.0672 (4)	0.5794 (4)
C(8)	0.4288 (4)	0.2317 (3)	0.1430 (2)	C(64)	1.0595 (5)	-0.0237 (4)	0.6332 (4)
C(9)	0.5340 (4)	0.2030 (3)	0.1600 (2)	C(65)	1.0178 (6)	0.0866 (5)	0.6710 (3)
C(10)	0.5811 (4)	0.1553 (3)	0.1255 (2)	C(66)	0.9479 (7)	0.1490 (4)	0.6590 (3)
C(11)	0.6844 (4)	0.1322 (3)	0.1368 (2)	C(71)	0.6435 (5)	-0.1518 (4)	0.5035 (3)
C(12)	0.7381 (4)	0.0949 (3)	0.0950 (2)	C(72)	0.6408 (5)	-0.1622 (3)	0.5685 (3)
C(13)	0.8399 (4)	0.0903 (3)	0.1189 (2)	C(73)	0.6289 (5)	-0.1041 (3)	0.6568 (3)
C(14)	0.8510 (4)	0.1234 (3)	0.1764 (2)	C(74)	0.6167 (5)	-0.0315 (4)	0.6826 (3)
C(15)	0.9465 (4)	0.1355 (3)	0.2136 (2)	C(75)	0.7020 (6)	0.0774 (4)	0.7055 (3)
C(16)	0.9585 (4)	0.1767 (3)	0.2654 (2)	C(76)	0.8063 (6)	0.1136 (4)	0.7100 (3)
C(17)	1.0576 (4)	0.1871 (3)	0.3030 (2)	C(81)	0.7279 (6)	-0.0918 (4)	0.4315 (3)
C(18)	1.0401 (4)	0.2318 (3)	0.3465 (2)	C(82)	0.6568 (6)	-0.0288 (5)	0.4184 (3)
C(19)	0.9284 (4)	0.2488 (3)	0.3361 (2)	C(83)	0.6351 (6)	0.0905 (5)	0.4411 (3)
C(20)	0.8814 (4)	0.2944 (3)	0.3728 (2)	C(84)	0.6934 (7)	0.1525 (5)	0.4702 (4)
C(21)	0.4231 (4)	0.3591 (3)	0.2914 (2)	C(85)	0.7717 (7)	0.2004 (4)	0.5620 (4)
C(22)	0.4207 (5)	0.4309 (3)	0.2798 (3)	C(86)	0.7762 (7)	0.1935 (4)	0.6275 (4)
C(23)	0.3320 (5)	0.4712 (3)	0.2830 (3)	N(1)	0.6996 (3)	0.2850 (2)	0.3204 (2)
C(24)	0.2443 (5)	0.4386 (4)	0.2994 (3)	N(2)	0.5793 (3)	0.2309 (2)	0.2133 (2)
C(25)	0.2461 (5)	0.3670 (4)	0.3112 (3)	N(3)	0.7552 (3)	0.1476 (2)	0.1863 (2)
C(26)	0.3340 (5)	0.3271 (3)	0.3073 (2)	N(4)	0.8808 (3)	0.2144 (2)	0.2868 (2)
C(31)	0.5131 (4)	0.1289 (3)	0.0709 (2)	N(5)	0.7406 (4)	-0.1171 (3)	0.4912 (2)
C(32)	0.5006 (5)	0.1674 (3)	0.0190 (2)	N(6)	0.8361 (5)	0.1316 (3)	0.6522 (3)
C(33)	0.4344 (5)	0.1427 (3)	-0.0317 (3)	O(1)	0.6270 (3)	0.1179 (2)	0.2968 (2)
C(34)	0.3812 (5)	0.0799 (4)	-0.0294 (3)	O(2)	0.7344 (3)	0.1103 (2)	0.3219 (2)
C(35)	0.3938 (6)	0.0414 (4)	0.0228 (3)	O(3)	0.9459 (3)	-0.0873 (2)	0.5595 (2)
C(36)	0.4589 (5)	0.0666 (4)	0.0718 (3)	O(4)	1.0023 (3)	0.0394 (2)	0.6212 (2)
C(41)	1.0444 (4)	0.1047 (3)	0.1962 (2)	O(5)	0.6385 (3)	-0.0952 (2)	0.5964 (2)
C(42)	1.1287 (5)	0.1475 (3)	0.1887 (3)	O(6)	0.7087 (3)	0.0090 (2)	0.6801 (2)
C(43)	1.2198 (5)	0.1179 (4)	0.1728 (3)	O(7)	0.6993 (3)	0.0296 (3)	0.4539 (2)
C(44)	1.2255 (5)	0.0459 (4)	0.1632 (3)	O(8)	0.7100 (4)	0.1446 (2)	0.5326 (2)
C(45)	1.1419 (5)	0.0028 (3)	0.1695 (3)	K	0.7867 (1)	0.0075 (1)	0.5728 (1)
C(46)	1.0522 (4)	0.0322 (3)	0.1864 (3)	Mn	0.7139 (1)	0.1877 (0)	0.2693 (0)
C(51)	0.9524 (4)	0.3296 (3)	0.4212 (2)				
C(52)	1.0280 (5)	0.3779 (3)	0.4099 (3)				

[a] Numbers in parentheses following atomic coordinates are estimated standard deviations.

Table VIII. Selected Bond Lengths (Å) for $[MnTPPO_2][K(K222)]$[a]

O1-O2	1.421 (5)	C4-C5	1.385 (7)	C12-C13	1.343 (7)
Mn-O1	1.901 (4)	C4-N1	1.368 (6)	C13-C14	1.451 (7)
Mn-O2	1.888 (4)	C5-C6	1.406 (7)	C14-C15	1.403 (7)
Mn-N1	2.202 (4)	C6-C7	1.433 (7)	C14-N3	1.370 (6)
Mn-N2	2.151 (4)	C6-N2	1.373 (7)	C15-C16	1.412 (7)
Mn-N3	2.199 (4)	C7-C8	1.351 (7)	C16-C17	1.439 (7)
Mn-N4	2.184 (4)	C8-C9	1.455 (7)	C16-N4	1.382 (6)
C1-C2	1.455 (7)	C9-C10	1.401 (7)	C17-C18	1.355 (7)
C1-C20	1.404 (7)	C9-N2	1.378 (6)	C18-C19	1.458 (7)
C1-N1	1.369 (6)	C10-C11	1.386 (7)	C19-C20	1.408 (7)
C2-C3	1.342 (7)	C11-C12	1.454 (7)	C19-N4	1.366 (6)
C3-C4	1.455 (7)	C11-N3	1.374 (6)		
K-O3	2.774 (4)	K-O6	2.814 (4)	K-N5	3.007 (5)
K-O4	2.889 (4)	K-O7	2.823 (4)	K-N6	2.974 (5)
K-O5	2.832 (4)	K-O8	2.866 (5)		

[a] Estimated standard deviations in parentheses.

O_2^{2-} in an eclipsed conformation.

The O–O bond distance in **1**, 1.421 (5) Å, falls between those of $MoTTP(O_2)_2$ (1.399 (6) Å)[24] and $TiOEPO_2$ (1.445 (5) Å)[23] and is typical of metal-peroxo complexes in general.[22] It is outside the range of O–O distances (approximately 1.25 Å) in metal-superoxo complexes.[22] The Mn–O distances are nearly identical, 1.901 (4) and 1.888 (4) Å, while the perpendicular distance from the manganese atom to the O–O midpoint is 1.76 Å. Of particular interest is the displacement of the Mn atom from the least-squares plane based on the four pyrrole nitrogen atoms. This displacement, 0.764 Å, is extraordinarily large for a manganese(III)-porphyrin, approximately 0.5 Å greater than that for other structurally characterized manganese(III)-porphyrin complexes (see Table VI). The Mn–N bond distances in **1**, which average 2.184 (23) Å, are also unusually long. Manganese(III)-porphyrin complexes typically are found to have Mn–N distances on the order of 2.01 Å (see Table VI).

The two Mn–N bonds eclipsed by the peroxo ligand are significantly shorter than the other two (2.153 (4) and 2.184 (4) vs. 2.199 (4) and 2.202 (4) Å). This is the reverse of the situation for the $TiOEPO_2$[23] complex, where the Ti–N bonds eclipsed by the peroxo ligand are longer than the other two. Another asymmetry that appears to be related to the peroxo ligand is the location of N2 and N4, eclipsed by the peroxo ligand, 0.074 Å below the least-squares plane based on the four nitrogen atoms, relative to that of N1 and N3, which are 0.074 Å above the plane. This distortion is also reflected in the N2–Mn–N4 and N1–Mn–N3 angles of 134.5° (2) and 143.5° (2), respectively. A similar distortion is seen in **2**, but it is significantly smaller (compare Figures 2 and 4). The porphyrin core of **1** has a domed configuration with the Mn atom and the four nitrogen atoms above the mean porphyrin plane. A similar shape is observed for **2**, but the out-of-plane displacements are again smaller (compare Figures 2 and 4).

As with **2**, the counterion to the Mn peroxo anion is the potassium cation chelated by a cryptate (K222). The cryptate is used because it increases the solubility of KO_2 in THF and because its large size makes it a good counterion for crystallization of porphyrin anions. The bond distances (see Table VII) are similar to those of **2** and other structurally characterized complexes.[21] The average cryptate bond distances are as follows: K–O = 2.833

(24) Chevrier, B.; Diebold, T.; Weiss, R. *Inorg. Chim. Acta* **1976**, *19*, L57.

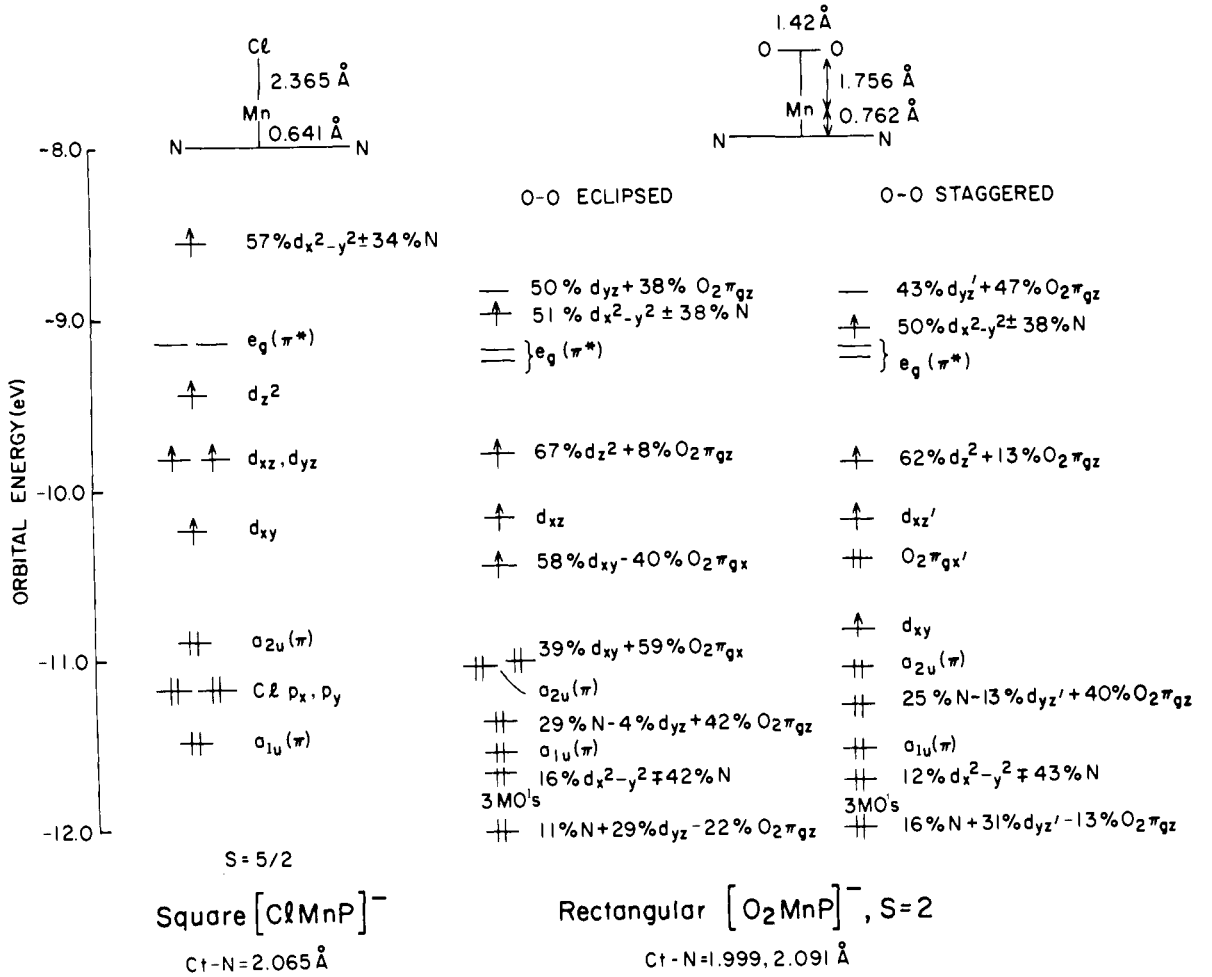

Figure 7. IEH calculated orbital energies of [Mn^{II}PCl]$^-$, left; [Mn^{III}PO$_2$]$^-$ with the O_2 eclipsed, center; and [Mn^{III}PO$_2$]$^-$ with the O_2 staggered with respect to the pyrrole nitrogens, right. [Mn^{II}PCl]$^-$ was calculated with a square porphine, the [Mn^{III}PO$_2$]$^-$ species with rectangular porphines (see Table II for coordinates). The *x* and *y* axis lie along the pyrrole nitrogens for all the complexes. For convenience, primed labels have been used for certain orbitals of the staggered form of [Mn(III)PO$_2$]$^-$: the d_{xz}' corresponds to ($d_{xz} - d_{yz}$), the d_{yz}' to ($d_{xz} + d_{yz}$), and the $O_2\pi_{gx}'$ to ($O_2\pi_{gx} - O_2\pi_{gy}$).

(40), K-N = 2.991 (23), C-C = 1.500 (15), C-O = 1.422 (11), C-N = 1.468 (16) Å.

MO Description. Figure 7 shows the results of IEH calculations on [Mn^{II}PCl]$^-$ and [Mn^{III}PO$_2$]$^-$. The d orbitals of [Mn^{II}PCl]$^-$ assume a pattern typical[12c,27] for high-spin five-coordinate metalloporphyrins: $d_{xy} < d_{xz}, d_{yz} < d_{z^2} < d_{x^2-y^2}$. Little mixing occurs among the porphyrin π, the manganese d, and the chloride ligand orbitals. Each d orbital contains one electron since Mn(II) is d^5.

In contrast, the dioxygen and Mn d orbitals of [Mn^{III}PO$_2$]$^-$ mix strongly, causing a significant perturbation to the ordering. If we define the porphyrin plane as the *xy* plane and the *y* axis by the O–O axis, then the two highest filled orbitals of the O_2^{2-} moiety are the $O_2\pi_{gz}$ and the $O_2\pi_{gx}$. The $O_2\pi_{gx}$ mixes with the Mn d_{xy} to form hybrid $d_{xy} \pm O_2\pi_{gx}$ orbitals (for O–O eclipsing the pyrrole nitrogens, as in the structure of **1**). The $O_2\pi_{gz}$ mixes with the Mn d_{yz} to form hybrid $d_{yz} \pm O_2\pi_{gz}$ orbitals. The interaction between the $O_2\pi_{gz}$ and the d_{yz} is especially strong, causing a splitting of approximately 3eV between the bonding[28a] and the antibonding pairs (the tighter the Mn-O_2 bond, the larger the splitting). Thus the $d_{yz} + O_2\pi_{gz}$ antibonding orbital of [Mn^{III}PO$_2$]$^-$ lies 0.9 eV higher in energy than the unmixed d_{yz} orbital of [Mn^{II}PCl]$^-$.

The energy of the $d_{x^2-y^2}$ orbital depends upon the out-of-plane displacement of the Mn atom. The further the metal is out of plane, the lower the energy of the $d_{x^2-y^2}$ orbital because of weaker antibonding interactions with the pyrrole nitrogen lone pairs. Since the Mn is further out of plane for [Mn^{III}PO$_2$]$^-$ than for [Mn^{II}PCl]$^-$, the [Mn^{III}PO$_2$]$^-$ $d_{x^2-y^2}$ orbital occurs at a lower energy.

As a consequence of both these factors, i.e., large out-of-plane Mn displacement and strong d,$O_2\pi_g$ mixing, the d orbitals of [Mn^{III}PO$_2$]$^-$ display an unusual pattern: $d_{yz} - O_2\pi_{gz}$[28a] < 40% d_{xy} + 60% $O_2\pi_{gx}$[28b] < 60% d_{xy} − 40% $O_2\pi_{gx}$[28b] < $d_{xz} < d_{z^2} < d_{x^2-y^2} < d_{yz} + O_2\pi_{gz}$. The highest d orbital is no longer $d_{x^2-y^2}$ but a $d_{yz} + O_2\pi_{gz}$ hybrid. The peroxo-manganese(III) center formally contains eight electrons, four paired and four unpaired. Placing the four paired electrons into the two lowest orbitals and the four unpaired electrons into the next four orbitals leaves the $d_{x^2-y^2}$ singly occupied and the $d_{yz} + O_2\pi_{gz}$ empty. If one specifies the orbital occupancy such that the fourth electron is placed in the $d_{yz} + O_2\pi_{gz}$ rather than the $d_{x^2-y^2}$, the $d_{yz} + O_2\pi_{gz}$ orbital rises to 0.7 eV above the $d_{x^2-y^2}$. Thus a $(d_{xy} - O_2\pi_{gx})^1 (d_{xz})^1 (d_{z^2})^1 (d_{yz} + O_2\pi_{gz})^1$ configuration is clearly an excited state; the ground state of this d^4 complex is $(d_{xy} - O_2\pi_{gx})^1 (d_{xz})^1 (d_{z^2})^1 (d_{x^2-y^2})^1$. This orbital occupancy has important consequences for the NMR and optical spectra of **1**, to be discussed later.

The [MnPO$_2$]$^-$ calculations for **1** presented in Figure 7 were performed by using a rectangular porphyrin skeleton with effective C_{2v} symmetry, since the crystal structure of **1** shows the porphyrin to be significantly, rectangularly distorted in the solid state. Squaring of the porphyrin to effective D_{4h} symmetry produces only one noticeable difference in the MO's: the porphine $e_g(\pi^*)$ orbitals

(25) Scheidt, W. R.; Lee, Y. J.; Luangdilok, W.; Haller, K. J.; Anzai, K.; Hatano, K. *Inorg. Chem.* **1983**, *22*, 1516.
(26) Day, V. W.; Stults, B. R.; Tasset, E. L.; Marianelli, R. S.; Boucher, L. J. *Inorg. Nucl. Chem. Lett.* **1975**, *11*, 505.
(27) Gouterman, M.; Hanson, L. K.; Khalil, G.-E.; Leenstra, W. R.; Buchler, J. W. *J. Chem. Phys.* **1975**, *62*, 2343.

(28) (a) There is no single MO with pure $d_{yz} - O_2\pi_{gz}$ (bonding) character. Several MO's below the porphyrin $a_{2u}(\pi)$ contain d_{yz},$O_2\pi_{gz}$ and pyrrole nitrogen lone pair orbitals. (b) The d_{xy},$O_2\pi_{gx}$ hybrids arise when O-O eclipses a pyrrole nitrogen axis.

Table IX. Selected Bond Angles (deg) for $[MnTPPO_2][K(K222)]^a$

Mn-O1-O2	67.5 (2)		
Mn-O2-O1	68.5 (2)	C5-C4-N1	124.9 (5)
O1-Mn-O2	44.1 (2)	C4-C5-C6	125.5 (5)
O1-Mn-N2	90.0 (2)	C5-C6-N2	126.5 (5)
O2-Mn-N4	91.5 (2)	C5-C6-C7	124.1 (5)
N1-Mn-N3	143.5 (2)	C7-C6-N2	109.4 (5)
N2-Mn-N4	134.5 (2)	C6-C7-C8	108.7 (5)
N1-Mn-N2	83.0 (2)	C7-C8-C9	105.6 (5)
N2-Mn-N3	83.8 (2)	C8-C9-N2	110.1 (5)
N3-Mn-N4	82.6 (2)	C8-C9-C10	123.7 (5)
N4-Mn-N1	82.7 (2)	C10-C9-N2	126.2 (5)
C1-N1-Mn	125.8 (4)	C9-C10-C11	125.8 (5)
C1-N1-C4	107.0 (4)	C10-C11-N3	125.6 (5)
C4-N1-Mn	125.6 (4)	C10-C11-C12	124.9 (5)
C6-N2-Mn	125.5 (4)	C12-C11-N3	109.2 (5)
C6-N2-C9	106.3 (4)	C11-C12-C13	107.3 (5)
C9-N2-Mn	125.3 (4)	C12-C13-C14	107.1 (5)
C11-N3-Mn	125.0 (4)	C13-C14-N3	109.6 (5)
C11-N3-C14	106.8 (4)	C13-C14-C15	125.3 (5)
C14-N3-Mn	127.5 (3)	C15-C14-N3	124.9 (5)
C16-N4-Mn	124.4 (3)	C14-C15-C16	125.0 (5)
C16-N4-C19	106.6 (4)	C15-C16-N4	126.6 (5)
C19-N4-Mn	124.2 (3)	C15-C16-C17	123.5 (5)
C20-C1-N1	125.6 (5)	C17-C16-N4	109.9 (5)
C20-C1-C2	124.6 (5)	C16-C17-C18	107.1 (5)
C2-C1-N1	109.6 (5)	C17-C18-C19	107.0 (5)
C1-C2-C3	106.7 (5)	C18-C19-N4	109.5 (5)
C2-C3-C4	107.6 (5)	C18-C19-C20	122.9 (5)
C3-C4-N1	109.1 (5)	C20-C19-N4	127.6 (5)
C3-C4-C5	125.8 (5)	C19-C20-C1	124.2 (5)

[a] Estimated standard deviations in parentheses.

become degenerate (these are split by 0.06 eV in the C_{2v} case). Coefficients agree to within 2%.

O–O Orientation and Macrocycle Distortion. The question arises as to why the dioxygen of **1** eclipses a pyrrole nitrogen axis. A comparison of the IEH calculations presented in Figure 7 for $[Mn^{III}PO_2]^-$ with eclipsed vs. staggered peroxide conformations shows only one major difference: the d_{xy} and $O_2\pi_{gx}$ orbitals of the eclipsed species form bonding and antibonding d_{xy},$O_2\pi_{gx}$ hybrids whereas they remain unmixed for the staggered species. Ellinger et al.,[29] rationalizing the eclipsed structure of $TiOEPO_2$,[23] suggested that an eclipsed conformation will be stable if the bonding $d_{xy} + O_2\pi_{gx}$ hybrid contains more oxygen character than the antibonding $d_{xy} - O_2\pi_{gx}$ hybrid and if the bonding hybrid lies at lower energy than the unmixed $O_2\pi_{gx}$. The IEH calculations on $[MnPO_2]^-$ are consistent with this view. The doubly occupied orbital of the eclipsed form is $40\%d_{xy} + 60\%O_2\pi_{gx}$ and lies 0.6 eV below the unmixed $O_2\pi_{gx}'$ of the staggered form.

The IEH calculations do not yield a simple rationalization for the rectangular distortion of the porphyrin ring of **1**. Furthermore, a comparison of the structures of **1** and $TiOEPO_2$[23] reveals that, although the eclipsed peroxide ligand causes a rectangular distortion in both, for **1**, the O–O binds along the short N···N axis, whereas for $TiOEPO_2$, the O–O binds along the long N···N axis. INDO calculations were therefore performed on $[Mn^{III}PO_2]^-$ and $Ti^{IV}PO_2$ to investigate further this phenomenon. Figures 8 and 9 give plots of the total energy as a function of O–O orientation for $[Mn^{III}PO_2]^-$ and $Ti^{IV}PO_2$, respectively.

$[Mn^{III}PO_2]^-$ was calculated with both a square and a rectangular porphyrin ring. The square porphine gives an essentially flat curve. The rectangular porphine exhibits a minimum for O–O along the short N···N axis, with the curve rising steadily to a maximum for O–O along the long N···N axis. Surprisingly, in light of the conclusions drawn from the IEH calculations, there is no additional barrier at 45° for a staggered O–O configuration.

The energy minimum for $Ti^{IV}PO_2$ occurs for O–O along the long rather than the short N···N axis. The difference in energy between the two axes is smaller than for rectangular $[Mn^{III}PO_2]^-$, but the porphine distortion is also smaller. The shape of the

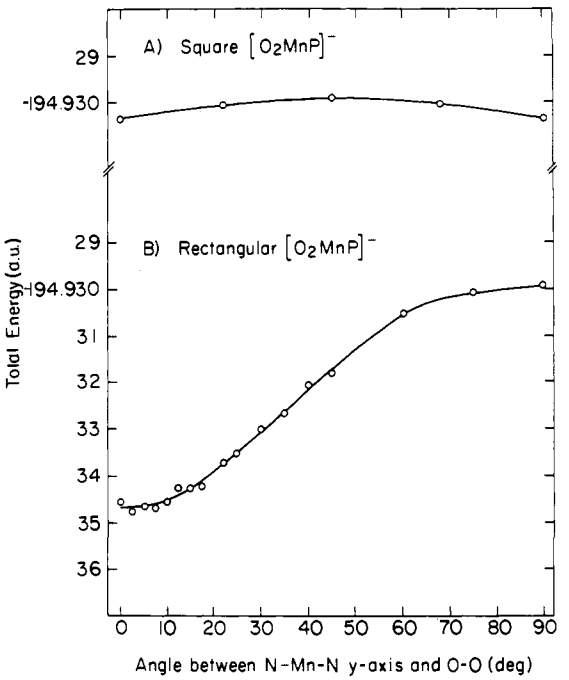

Figure 8. Total energy (in au) from INDO calculations on $[Mn^{III}PO_2]^-$ plotted as a function of O–O orientation above the porphyrin plane. In curve A the porphine macrocycle is square (D_{4h} symmetry), and in curve B the porphine is rectangularly distorted (C_{2v}). For a given curve the only variable is the angle between the O–O and N···N axes. For curve B, 0° represents O–O alignment along the short N···N axis as found for **1** and 90° alignment along the long N···N axis; 0.01 au = 3 kcal.

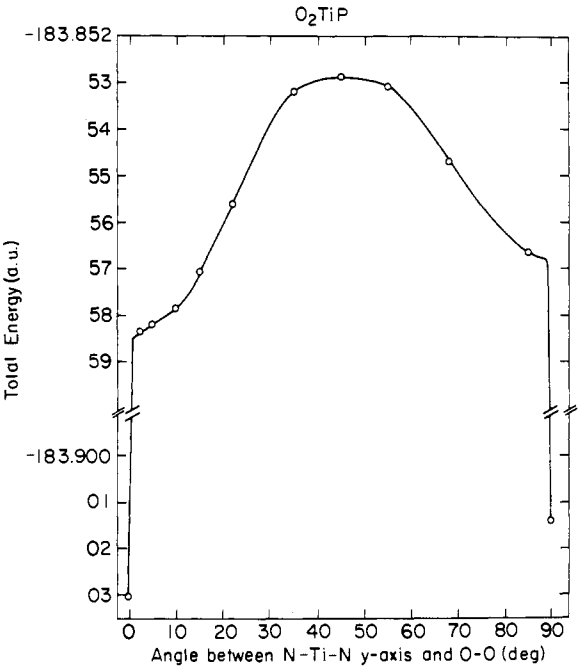

Figure 9. Total energy (in au) from INDO calculations on $Ti^{IV}PO_2$ plotted as a function of O–O orientation above the porphyrin plane. For this molecule, 0° represents O–O alignment along the long N···N axis, as found in the structure of $TiOEPO_2$[22] and 90° alignment along the short N···N axis. The following distances were used in these calculations: O–O = 1.445, Ti–Ct = 0.62, Ti–O = 1.825, and Ti–N = 2.128, 2.090 Å.

$Ti^{IV}PO_2$ curve differs substantially from the shape of the $[Mn^{III}PO_2]^-$ curves. Consistent with a previous calculation on this system,[30] the maximum occurs at 45° (staggered O–O). The

(29) Ellinger, Y.; Latour, J.-M.; Marchon, J.-C.; Subra, R. *Inorg. Chem.* **1978**, *17*, 2024.

(30) Rohmer, M.-M.; Barry, M.; Dedieu, A.; Veillard, A. *Int. J. Quant. Chem.: Quant. Biol. Symp.* **1977**, *4*, 337.

Table X. Known and Proposed Metalloporphyrin Superoxide and Peroxide Adducts

ligand	complex	reaction	characterization	ref
superoxo	$FTiTPPO_2$	$FTiTPP + O_2$	ESR $g = 2.009$	31
	$CrTPPO_2$	$CrTPP + O_2$	IR ν O–O = 1142 cm^{-1} stoichmtry of O_2 uptake	32
	$pyCoTPPO_2$	$pyCoTPP + O_2$	ESR $g = 1.79, 3.285$	33
	$ZnTPPO_2^-$	$ZnTPP + O_2^-$	ESR $g = 2.07$	34
	$BFeTpivPPO_2$[a]	$BFeTpivPP + O_2$	structure: O–O bond dist 1.26 Å IR ν O–O = 1163 cm^{-1}	1
peroxo	$TiTPPO_2$	$OTiTPP + H_2O_2$	structure: O–O bond dist 1.445 Å IR ν O–O = 898 cm^{-1}	23
	$MoTTP(O_2)_2$	$O(OH)MoTPP + H_2O_2$	structure: O–O bond dist 1.399 Å IR ν O–O = 964 cm^{-1}	24
	$MnTPPO_2$	$MnTPP + O_2$	ESR $g = 1.45, 2, 5.4$ IR ν O–O = 983 cm^{-1}	35 36
	$FeTPPO_2^-$	$FeTPP + O_2^-$	ESR $g = 2, 4.2, 8$ IR ν O–O = 806 cm^{-1}	2
	$MnTPPO_2^-$	$MnTPP + O_2^-$	structure: O–O bond dist 1.421 Å	this work

[a] B = *N*-methylimidazole.

curve looks like a lopsided bell centered at 45° until it reaches the N···N axes. At both axes, the energies plunge.

As found for the IEH calculations, the INDO calculations do not reveal the factors which lead to the rectangular distortion and preferred O–O orientations of **1** and $Ti^{IV}OEPO_2$. However, they do predict minimum energy conformations for both $[Mn^{III}PO_2]^-$ and $TiPO_2$ that agree with the observed solid-state structures.

NMR spectra[8,23b] of both complexes show that in solution at room temperature the dioxygen is not locked into position but is freely rotating above the plane of the macrocycle with concomitant averaging of the porphyrin skeleton. For TiO_2 porphyrins, the barrier to rotation of the O–O moiety has been determined experimentally and is approximately 10 kcal/mol.[23b] The calculations compare favorably; the INDO method predicts 15 kcal/mol, and previous ab initio calculations[30] predicted 5 kcal/mol. In contrast, the barrier calculated for $[MnPO_2]^-$ is an order of magnitude smaller, 1.4 kcal/mol, suggesting that a freezing out of the O–O motion above the macrocycle will occur at much lower temperatures for peroxo-manganese(III)-porphyrin complexes.

Discussion

Metalloporphyrin–dioxygen complexes fall into two categories based on the O_2 formal oxidation state: those complexes in which the dioxygen ligand is best described as superoxide-like and those in which it best described as peroxide-like. These complexes are summarized and described in Table X.

The manganese–peroxo complex **1** was originally prepared by Valentine and Quinn[7] by reaction of 2 equiv of superoxide with $Mn^{III}TPP^+$ in Me_2SO. It was originally believed to be $[Mn^{II}TPP(O_2^-)]^-$, because it lacked the split Soret band in the visible spectrum that is usually associated with manganese(III)-porphyrins.[37] Shirazi and Goff[8] later provided additional support for this assignment based on a deuterium NMR study of **1** in which they observed the large downfield contact shifts of pyrrole deuterium signals characteristic of a singly occupied manganese $d_{x^2-y^2}$ orbital. They concluded on this basis that **1** must contain Mn(II) rather than Mn(III) since that orbital is unoccupied in typical high spin d^4 Mn(III) complexes.

The results of the X-ray crystal structural study of **1** indicate that the peroxide ligand has an O–O bond distance and a symmetrical bidentate mode of binding to the manganese atom that is diagnostic of a peroxo complex. These results led to the inescapable conclusion that **1** contains Mn(III) rather than Mn(II). This conclusion seems to be in direct conflict with several experimental observations. These are (1) the downfield NMR shifts indicating single occupancy of the $d_{x^2-y^2}$ orbital,[8] which is expected to be unoccupied in Mn(III) complexes, (2) the abnormally long Mn–N bonds and large out-of-plane displacement of the Mn atom from the porphyrin plane compared to other Mn(III) complexes, and (3) the absence in the visible spectrum of the split Soret band that is typical of manganese(III)-porphyrin complexes.

Observations 1 and 2 can be rationalized in simple crystal field terms if it is assumed that the large out-of-plane displacement of the manganese atom and the dinegative charge on the peroxo ligand result in an energy level scheme in which the energy of the d_{yz} orbital (see Figure 7) exceeds that of the $d_{x^2-y^2}$ orbital. Molecular orbital calculations provide both quantitative support for this hypothesis and additional insight into the nature of the metallo–peroxo interaction.

Hanson and Hoffman[38] have successfully applied IEH calculations to $MnTPPO_2$, an adduct of $Mn^{II}TPP$ and dioxygen. Seemingly contradictory optical and EPR spectra were found to be consistent with the molecular orbital pattern calculated for a manganese(IV)porphyrin–peroxo complex, with O–O bound in a bidentate fashion parallel to the porphyrin plane. In the present investigation similar IEH calculations performed on $[Mn^{III}TPP-O_2]^-$ reconcile the spectroscopic and crystallographic data of **1**.

NMR and Optical Spectra. Two factors, the tight manganese–peroxide bonding and the large Mn out-of-plane displacement, lead to an alteration of the normal d orbital ordering. As shown in Figure 7, the highest energy d orbital is a $d_{yz} + O_2\pi_{gz}$ hybrid not the $d_{x^2-y^2}$. Complex **1** is therefore predicted to be high spin d^4 with a singly occupied $d_{x^2-y^2}$ orbital, a result consistent with Shirazi and Goff's[8] observation of downfield NMR shifts for the pyrrole protons.

Manganese(III)-porphyrin complexes usually exhibit multiple Soret bands.[37] These are thought to arise from the presence of Mn $e_g(d_\pi)$, d_{xz} and d_{yz}, orbitals in the vicinity of the porphyrin $e_g(\pi^*)$.[27,39] Porphyrin a_{1u}, $a_{2u}(\pi) \rightarrow$ metal $e_g(d_\pi)$ charge-transfer transitions have the same symmetry as porphyrin a_{1u}, $a_{2u}(\pi) \rightarrow$ porphyrin $e_g(\pi^*)$ transitions. When the $\pi \rightarrow$ d charge-transfer and the $\pi \rightarrow \pi^*$ Soret transitions occur at comparable energies, they interact strongly to produce a "split Soret". In the $[Mn^{III}PO_2]^-$ case, however, orbitals of d symmetry are either too low (d_{xz}) or too high ($d_{yz} + O_2\pi_{gz}$) in energy for the mixing to occur. Thus the Soret band of **1** remains unperturbed. This contrasts with $Mn^{IV}TPPO_2$ which does exhibit multiple Soret bands.[35] Because the center of gravity of a d-orbital stack drops with increasing oxidation of the metal, the $d_{yz} + O_2\pi_{gz}$ hybrid

(31) Latour, J.-M.; Marchon, J.-C.; Nakajima, M. *J. Am. Chem. Soc.* **1979**, *101*, 3974.
(32) Cheung, S. K.; Grimes, C. J.; Wong, J.; Reed, C. A. *J. Am. Chem. Soc.* **1976**, *98*, 5028.
(33) Walker, F. A. *J. Am. Chem. Soc.* **1970**, *92*, 4235.
(34) Valentine, J. S.; Tatsuno, Y.; Nappa, M. *J. Am. Chem. Soc.* **1977**, *99*, 3522.
(35) (a) Hoffman, B. M.; Weschler, C. J.; Basolo, F. *J. Am. Chem. Soc.* **1976**, *98*, 5473. (b) Weschler, C. J.; Hoffman, B. M.; Basolo, F. *Ibid.* **1975**, *97*, 5278.

Table XI. Net Charge Densities (IEH Calculations)

	Mn	axial ligand	porphine ring	Mn–Ct[a] (Å)
$[Mn^{II}PCl]^-$	−0.01	−0.27	−0.72	0.64[c]
$Mn^{II}P$(pyridine)[b]	0.065	0.26	−0.325	0.51[d]
$Mn^{III}PCl$	0.12	−0.17	0.05	0.27[e]
$[Mn^{III}PO_2]^-$	0.04	−0.58	−0.46	0.76[c]
$Mn^{IV}PO_2$[b]	0.17	−0.54	0.37	0.51[f]

[a] Mn out-of-plane displacement. [b] Reference 38. [c] This work. [d] From Mn^{II}TPP(1-MeIm) structure, ref 14. [e] Reference 19. [f] Structure not determined. Value used in the calculations.

orbital of the Mn(IV) species lies just below the porphyrin $e_g(\pi^*)$ orbitals at an energy favorable for perturbing the optical spectra.[38]

Mn Displacement of 1. The 0.764-Å Mn out-of-plane displacement of **1** is the largest yet observed for a manganese–porphyrin and is significantly longer (approximately 0.5 Å) than values obtained for other Mn(III) complexes (see Table VI). Several factors may contribute to this unusually large displacement. Certainly major contributions come from the tight covalent π-bonding between the peroxide ligand and the Mn and the excess charge density on the "Mn(III)" center (described below).

Nonbonded atomic interactions may also play a role. O···N contacts influence the minimum approach of a peroxo ligand to the porphyrin ring. If the metal–O_2 interaction is stronger than the metal–porphyrin interaction, then the metal will compensate by moving out of plane. Although the distances of O1···N2 = 2.870 (6) and O2···N4 = 2.974 (6) Å for **1** are nearly equal to the "textbook" distance of 2.9 Å for O···N van der Waals contacts, shorter distances have been observed.

Tight π-bonding and O···N interactions appear to be the only major factors governing the out-of-plane displacement of $Ti^{IV}OEPO_2$, where charge density on the metal (Ti(IV), d^0) should have no influence. Here the O···N contacts are even shorter, 2.664 (5) and 2.667 (5) Å, with an out-of-plane displacement of 0.62 Å, the largest observed for a titanium–porphyrin.

Potentially short N···O distances, however, do not prohibit peroxo binding. In the case of $MoTTP(O_2)_2$,[24] Mo is forced to reside in the porphyrin plane due to the bis peroxo binding configuration. Even though there are more extreme N···O interactions (N···O distance of 2.46 Å, calculated by using data given in ref 24), MoTTP forms a stable complex with two peroxo ligands, even in the absence of out-of-plane displacement of the Mo.

Mn Displacement of 2 and Charge Densities. As discussed above, the peroxo ligand contribution to the 0.764-Å Mn out-of-plane displacement of **1** arises primarily from a combination of tight Mn–O_2 binding and possibly from nonbonded contacts between the peroxo oxygens and pyrrole nitrogens. These factors do not apply to the Mn of **2**, yet it is displaced 0.64 Å from the porphyrin plane, 0.13 Å more than the Mn of Mn^{II}TPP(1-methylimidazole).[14] The similarity of the Mn geometry for **1** and **2** is not surprising in light of the calculated charge densities. Table XI presents the net charge densities on the Mn, porphyrin ring, and axial ligand (L) for several MnPL complexes: negatively charged and neutral Mn(II), Mn(III), and Mn(IV). The Mn displacement of **2** may be due primarily to the anionic nature of the complex. Some of the excess negative charge is transferred to the Mn (compare $[Mn^{II}PCl]^-$ with the neutral $Mn^{II}P$(pyridine)). A more negative (or less positive) metal has a larger ionic radius. In addition, both the Cl^- ligand and the porphyrin ring of $[Mn^{II}PCl]^-$ are negatively charged and therefore electrostatically repulsive. A neutral $Mn^{II}PL$ complex, where L is an electron-donating ligand such a pyridine or 1-methylimidazole, has a positively charged ligand and a negatively charged ring.

Although the Mn atom of $[Mn^{III}PO_2]^-$ **1** is formally Mn(III), its charge density falls between that of $[Mn^{II}PCl]^-$ **2** and Mn^{II}TPP(pyridine). This suggests that the effective charge on the Mn atoms of **1** and **2** are similar. Table XI demonstrates that a formal description of oxidation state solely in terms of the MnL core ignores the contribution of the porphyrin ring. The porphyrin compensates much more for the charge of the axial ligand and the net charge of the complex than the Mn does. The excess charge density on the O_2^{2-} ligand relative to a Cl^- ligand comes mostly from the ring (compare either $[Mn^{III}PO_2]^-$ and $[Mn^{II}PCl]^-$ or $Mn^{IV}PO_2$ and $Mn^{III}PCl$). Similarly, the charge densities of $[Mn^{III}PO_2]^-$ and $Mn^{IV}PO_2$ or $[Mn^{II}PCl]^-$ and $Mn^{III}PCl$ demonstrate that the ring reflects the loss of an electron significantly more than does the metal, even though it is the metal which has been formally oxidized.

Conclusions

This work and previous work on $[MnTPPO_2]^-$ and $MnTPPO_2$ demonstrate that both complexes contain peroxo ligands bound side-on, parallel to the porphyrin plane. Furthermore, it is apparent that the peroxo ligand binds tightly to the metal and, in doing so, perturbs the Mn d orbitals in such a way that "typical" spectroscopic oxidation state markers become unreliable.

Acknowledgment. L.K.H. wishes to thank Jack Fajer for helpful discussions. This work was supported by a grant from the National Science Foundation (JSV), the National Institutes of Health (CES: GM-35329), and by the Division of Chemical Sciences, U.S. Department of Energy, under Contract No. DE-AC02-76CH00016 at BNL (L.K.H.).

Registry No. 1, 106266-47-1; **2**, 106335-75-5; Mn^{II}TPP, 31004-82-7.

Supplementary Material Available: Isotropic and anisotropic temperature factors and calculated hydrogen atom positions (8 pages); listing of structure factors for **1** and **2** (42 pages). Ordering information is given on any current masthead page.

(36) Urban, M. W.; Nakamoto, K.; Basolo, F. *Inorg. Chem.* **1982**, *21*, 3406.
(37) Boucher, L. J. *Ann. N.Y. Acad. Sci.* **1973**, *206*, 409.
(38) Hanson, L. K.; Hoffman, B. M. *J. Am. Chem. Soc.* **1980**, *102*, 4602.
(39) Hanson, L. K.; Eaton, W. A.; Sligar, S. G.; Gunsalus, I. C.; Gouterman, M.; Connell, C. R. *J. Am. Chem. Soc.* **1976**, *98*, 2672.